Publishing House
AKAPIT

COMPUTER METHODS IN MATERIALS SCIENCE
Informatyka w Technologii Materiałów

Vol. 20, 2020, No. 1

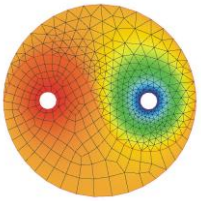

SPHERE PACKING ALGORITHM FOR THE GENERATION OF DIGITAL MODELS OF POLYCRYSTALLINE MICROSTRUCTURES WITH HETEROGENEOUS GRAIN SIZES

LUCYNA HAJDER*, ŁUKASZ MADEJ

AGH University of Science and Technology, al. Mickiewicza 30, 30-059 Krakow, Poland
**Corresponding author: hajder.lucyna@gmail.com*

Abstract

Development of the cellular automata (CA) sphere packing algorithm dedicated to the generation of two- and three-dimensional digital, synthetic microstructure models with heterogenous grain size distribution is presented within the paper. The synthetic microstructure model is generated in four major steps: generation of 2D/3D cellular automata computational domain, generation of circles/spheres with a required size distribution, close-packed filling of the computational domain with generated circles/spheres, growth of the circles/spheres according to the unconstrained CA growth algorithm. As a result, synthetic microstructure models with prescribed, e.g. uni- or bimodal, grain size distribution are obtained. To reduce the computational complexity and decrease execution time, the rotation of the circles/spheres during the packing stage is based on the vector accounting for the distance from computational domain borders and other spheres. The CA grain growth algorithm is also implemented using threads mechanism, allowing parallel execution of computations to increase its efficiency. The developed algorithm, along with the implementation details as well as a set of exemplary results, are presented within the paper.

Key words: DMR, Sphere Packing Algorithm, Cellular Automata

1. INTRODUCTION

Today, highly complex metallic materials that were previously reserved only for space exploration applications are becoming commonly applied in airplanes, cars, motorcycles, and even in more ordinary products such as electronics. Until recently, work on the development of those materials was carried out primarily through costly and time-consuming experimental and laboratory research. However, today's access to computing power creates new and often still unrecognized opportunities for materials science. Designing modern numerical models that accurately describe materials with respect to their actual microstructure with grains, phases, defects, or even atoms is a key stage in such a computer-aided material design. These digital material representation based (DMR) models have capabilities not only to recreate the morphology of microstructure but also to assign various material properties to subsequent micro-scale features (Madej, 2017). However, to properly replicate microstructure morphology in a digital sense, the sophisticated numerical algorithm has to be developed.

A DMR model can be created by the two conceptually different approaches. In the first concept, digital microstructure morphologies are recreated based on the experimental data acquired by, e.g., scanning electron microscopy electron backscattered diffraction technique SEM/EBSD (Raabe & Becker, 2000; Sitko et al., 2020), using complex algorithms for image and data analysis. Most of the times, the metallography investigation with light microscopy (LM) or electron microscopy (EM) is used to provide experimental data on microstructure state in the 2D space. For the 3D case, the serial sectioning

 ISSN 1641-8581

(Hoffpauir et al., 2007; Echlin et al., 2020) or tomographic methods, e.g., computed tomography (CT) or atom probe tomography (APT) are used depending on the type of material and size of the investigated volume (Banhart, 2008; Vásárhelyi et al., 2020). These approaches provide the exact representation of the investigated region; however, due to the required significant amount of experimental data, they are still considered as time-consuming and expensive. Therefore, the second concept is based on the generation of the synthetic models recreating microstructure state in a statistical manner with numerical algorithms, e.g., Voronoi tessellation, Monte Carlo Pots Model, etc. A detailed review of the topic can be found in (Madej, 2017).

A promising approach in the latter concept is the application of the circle/sphere/ellipse/ellipsoid packing algorithms (Jodrey & Tory, 1979; Visscher & Bolsterli, 1972; Orick et al., 2017; Romanova et al., 2020), generally referred here as sphere packing ones. This class of methods can be primarily divided into dynamic and constructive solutions. In the dynamic approaches, the spheres change their position or their size during the packing process, which is controlled by a shrinking algorithm (Tory & Jodrey, 1986; Torquato & Jiao, 2010; He et al., 2018), compression forces algorithm (Khirevich, et al., 2013; Baranau & Tallarek, 2014) or gravitational algorithm (Shi & Zhang, 2008; Hitti & Bernacki, 2013; Sahu, 2009; Ilina & Bernacki, 2016). In the case of constructive approaches, sphere parameters like size or position are preserved during the packing process, so they are less costly but have difficulties in achieving high-density packing (Evans, 1993; Cui & O'Sullivan, 2003; Kazakov et al., 2018).

The primary goal of these methods is to obtain a densely packed computational domain (Clarke & Wiley, 1987). However, the problem of precise control of spheres diameter to obtain heterogeneous microstructure morphologies with required size distribution is equally important and, therefore, is addressed within the current work.

The gravitational sphere packing method was selected for the investigation as an efficient algorithm that has the capability of generating complex microstructure morphologies using densely packed particles. A series of modifications were developed and introduced to the classical algorithm in order to provide the possibility for computationally efficient generation of microstructure morphologies with controlled non-homogeneous grain size distribution. Finally, to provide a realistic representation of grain boundary geometry, the sphere packing algorithm was combined with the cellular automata grain growth model.

2. MATHEMATICAL MODEL OF THE SPHERE PACKING ALGORITHM

The synthetic digital microstructure is generated in the developed approach within five major steps. The first is responsible for the generation of the 2D/3D computational domain in the form of cube, square, rectangle or cuboid, as seen in figure 1.

In this case, from the definition of the computational domain, its origin is in the (0,0,0) point, which is located in the left bottom corner, and spreads to the right top corner located in (*n*,*m*,*o*) point. Then during the second step of the algorithm, a generation of circles/spheres with required size distribution is realized. These circles/spheres are defined by their id number, centroid point, and radius r, as seen in figure 2 for the 3D and 3D space, respectively. Specific radii are generated according to the defined size distribution. Three different options have been investigated in this case: the unimodal, bimodal and trimodal (figure 3).

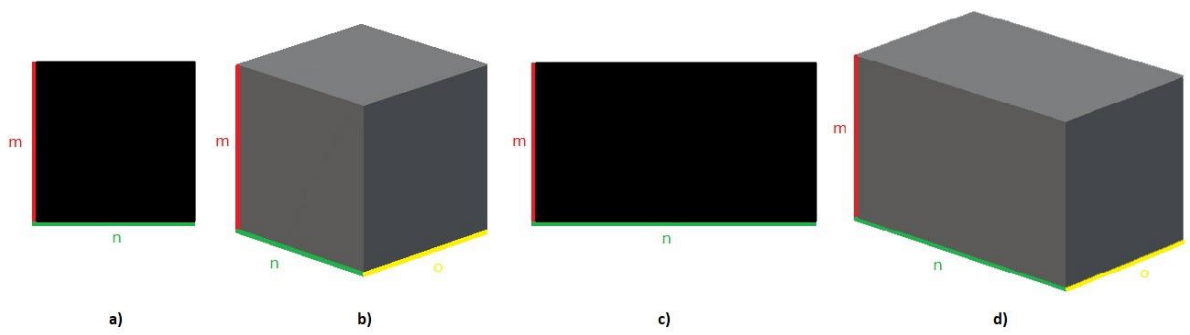

Fig. 1. *Investigated geometries of computational domain: a) square with size n×m, b) cube with size n×m×o o, c) rectangle with size n×m and d) cuboid with size n×m×o.*

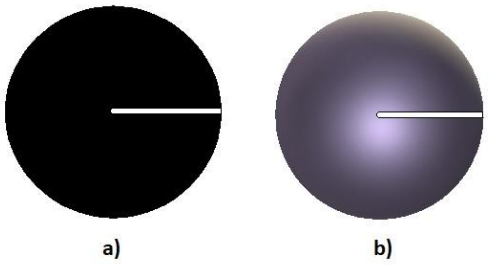

Fig. 2. *Definition of a) circle, b) sphere with defined radius.*

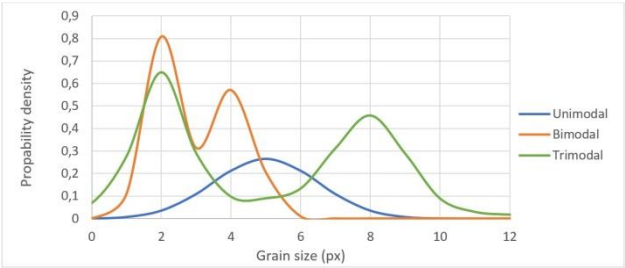

Fig. 3*. Grain size distribution functions: unimodal, bimodal and trimodal.*

Then, during the third step of the developed algorithm subsequent circles/spheres are initially located at the top of the computational domain as seen in figure 4, and are then subjected to the algorithm responsible for their downward movement until impingement that prevails further changes in the position. The algorithm is based on a series of steps dealing with defined different events that can occur during the movement of an investigated shape.

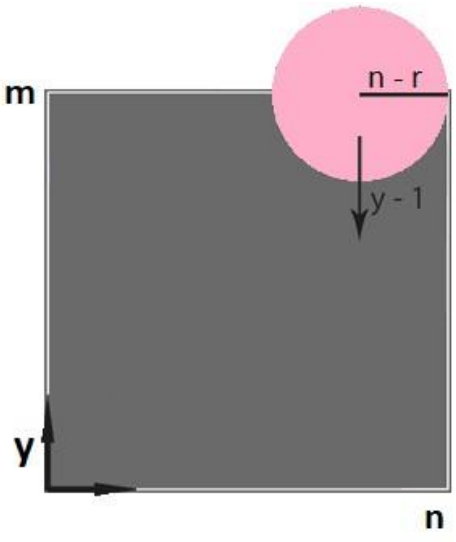

Fig. 4*. Computational domain with an initial position of the generated shape (circle case study).*

In this case, in each iteration the y position of the centre of the ith moving shape is translated vertically by $dy = 0.05r_i$ until:

$$y_i \geq r_i \tag{1}$$

To verify that the new position does not collide with neighbouring shapes, the following expression is used:

$$\left(r_i + r_j\right)^2 \geq \left(x_i - x_j\right)^2 + \left(y_i - y_j\right)^2 \tag{2}$$

where: x_i, y_i – coordinates of the 2D moving shape, r_i – radius of the 2D shape, r_j, x_j, y_j, are corresponding parameters for all neighbouring, stationary shapes N, $j \in [1,N]$.

If the collision is identified, then the investigated shape is translated to the sides, and several cases are considered as schematically shown in figure 5 and figure 6.

The rotation after collision results in a change in the x_i and y_i values:

$$x_i = x_i \pm dx \tag{3}$$

$$y_i = \sqrt{\left(r_j + r_i\right)^2 - \left(x_j - x_i\right)^2} + y_j \tag{4}$$

where: $dx = 0{,}01r$.

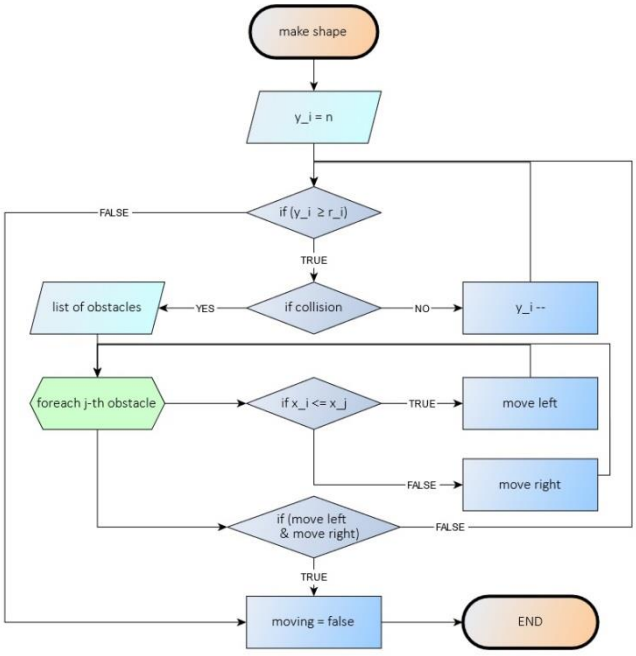

Fig. 5*. Flow chart for the shape movement algorithm in the 2D space.*

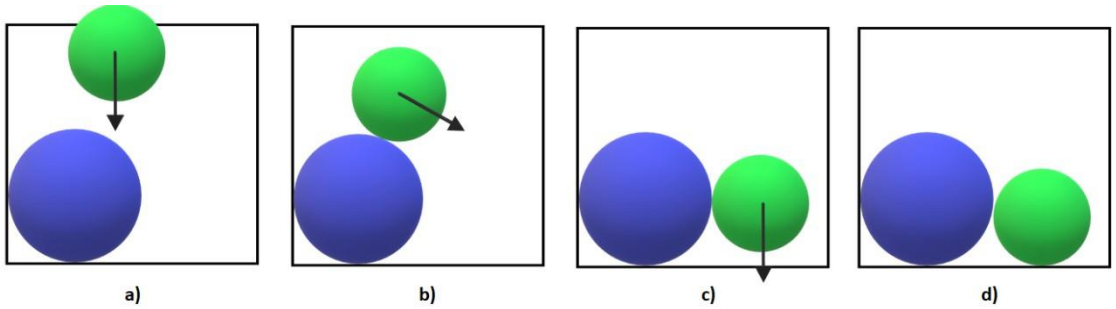

***Fig. 6**. Flow chart for the shape movement algorithm in the 2D space.*

When the circle becomes stationary, its parameters are saved into the list of stationary shapes. This algorithm is performed until the computational domain is unable to accommodate more shapes.

Capabilities of the developed model were tested on the basis of three case studies for different size distributions, as shown in table 1. Examples of obtained results for the computational domain with the 550×300 px are presented in figure 7, figure 8 and figure 9.

***Table 1.** Parameters for the three case studies of the developed 2D version of the algorithm.*

Distribution	Range of radius, px	m, px	σ, px	Packing density, %
Unimodal	[1; 15]	8	3	77.01
Bimodal	[1; 5] [10; 15]	3 12	1 3	78.16
Trimodal	[1; 3] [5; 9] [12; 15]	2 7 13	1 3 1	77.78

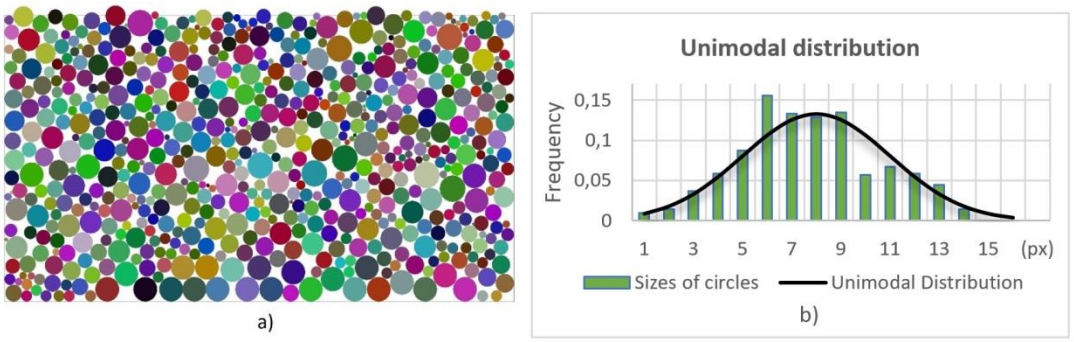

***Fig. 7**. Results for the unimodal distribution: a) packed computational domain, b) comparison of the theoretical and obtained size distributions.*

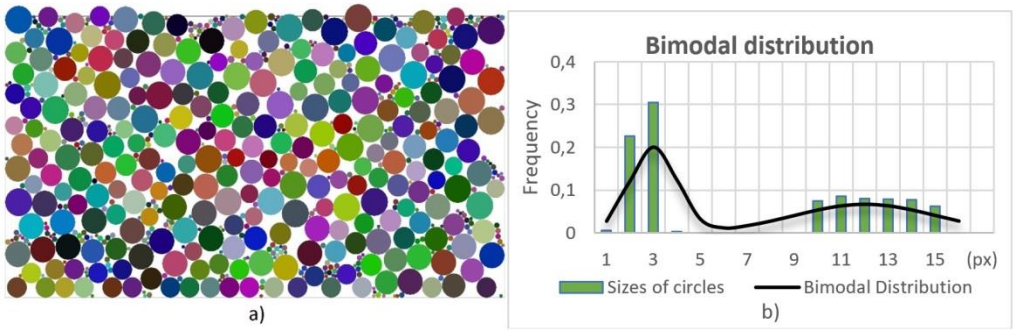

***Fig. 8**. Results for the bimodal distribution: a) packed computational domain, b) comparison of the theoretical and obtained size distributions.*

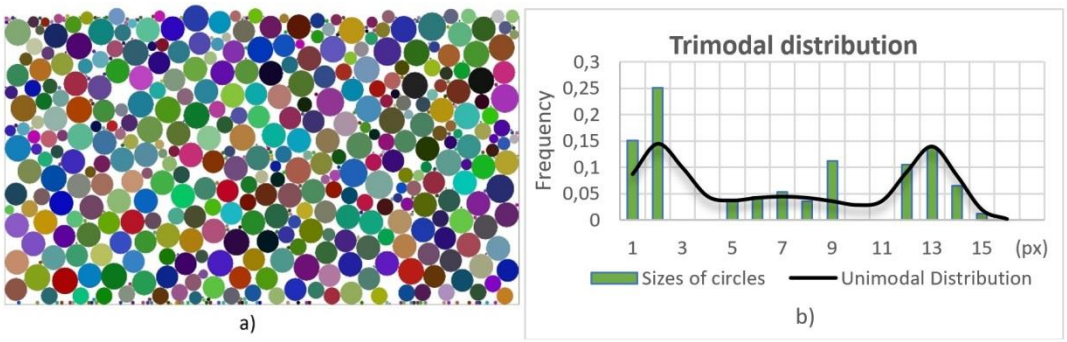

***Fig. 9**. Results for the trimodal distribution: a) packed computational domain, b) comparison of the theoretical and obtained size distributions.*

As presented, the developed algorithm provides results with required size distribution for simple unimodal as well as multimodal cases. Results are a good representation of the theoretical size distribution with just a slight discrepancy. The packing density in these 2D models is at the level above 77%.

The same algorithm is also adapted to the 3D space with the shapes represented by spheres. However, in this case, aside from x and y, also the z coordinate is taken into account. Therefore, the collision event is identified by the following equation:

$$(r_1 + r_2)^2 \geq (x_1 - x_2)^2 + (y_1 - y_2)^2 + (z_1 - z_2)^2 \qquad (5)$$

The sideways movement to relocate the centre of the sphere after the collision is controlled by:

$$dx = \frac{\sum_{i=0}^{n}(x_1 - x_i)}{n} \qquad (6)$$

$$dy = \frac{\sum_{i=0}^{n}(y_1 - y_i)}{n} \qquad (7)$$

$$dz = \frac{\sum_{i=0}^{n}(z_1 - z_i)}{n} \qquad (8)$$

Capabilities of the developed model were again tested on the basis of three case studies from table 2. The size of the computational domain was assumed to be 550×300×150 px. Examples of obtained results are presented in figure 10, figure 11 and figure 12.

***Table 2**. Parameters for the three case studies of the developed 3D version of the algorithm.*

Distribution	Range of radius, px	m, px	σ, px	Packing density, %
Unimodal	[1; 15]	7	3	45.73
Bimodal	[1; 6] [10; 15]	3 12	3 1	45.9
Trimodal	[1; 3] [5; 9] [12; 15]	2 7 13	1 3 1	45.49

In the 3D case studies, the packing density is reduced to approx. 45%. Unfortunately, the lower the packing density, the higher the deviation from the required size distribution after the subsequent cellular automata grain growth stage is expected.

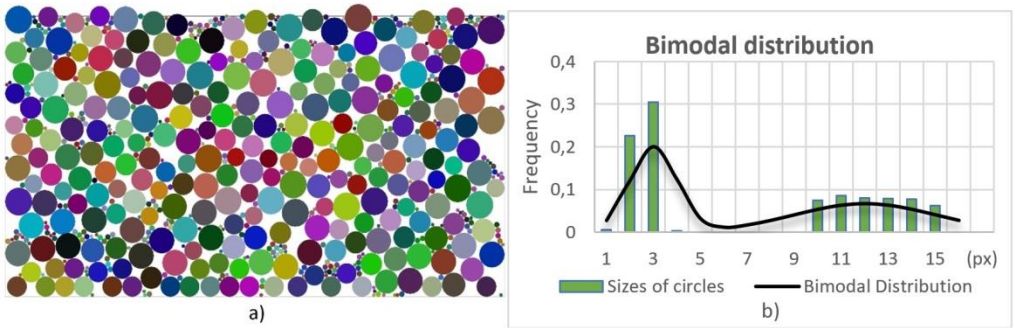

***Fig. 10**. Results for the unimodal distribution: a) packed computational domain, b) comparison of the theoretical and obtained size distributions.*

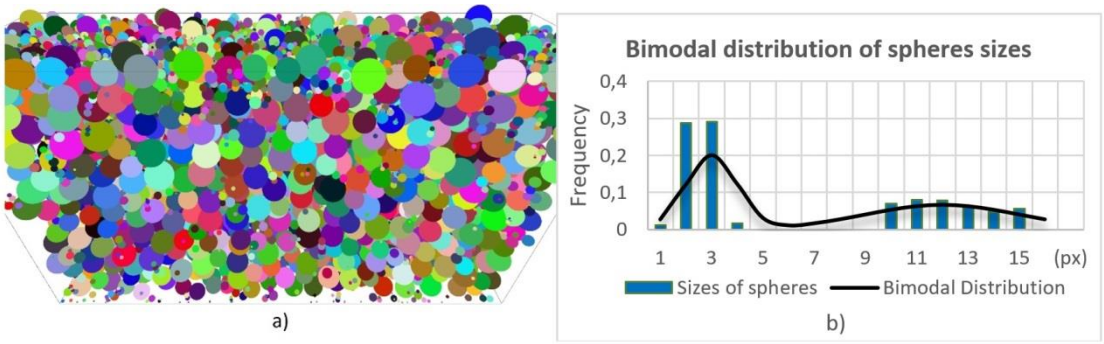

***Fig. 11**. Results for the bimodal distribution: a) packed computational domain, b) comparison of the theoretical and obtained size distributions.*

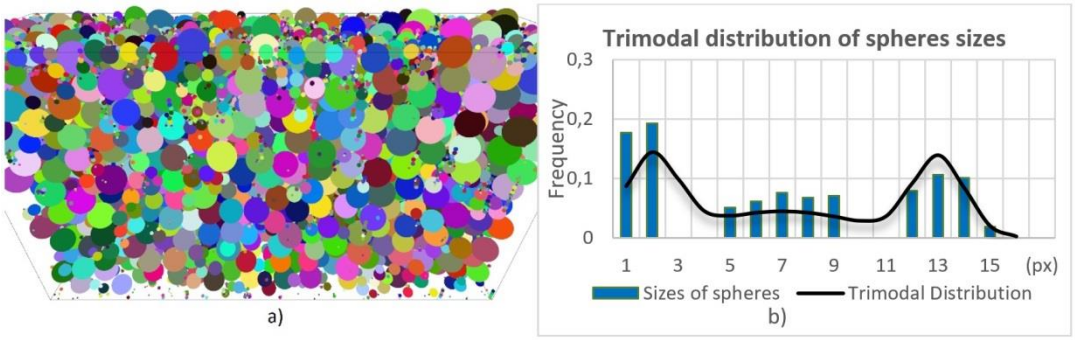

***Fig. 12**. Results for the trimodal distribution: a) packed computational domain, b) comparison of the theoretical and obtained size distributions.*

3. CELLULAR AUTOMATA GRAIN GROWTH ALGORITHM

The creator of Cellular Automata (CA) is J. von Neumann, who in the early 1960s used them to describe processes relevant to the phenomenon of replication of living organisms (Von Neumann, 1966). Later, this method became very popular in various fields of science and technology, including material science (Raabe & Becker, 2000).

The cellular domain is described by means of a regular grid of cells. Each CA cell has an id number and a specified type of neighbourhood. The id number is used to represent CA cells belonging to the same grain in the polycrystalline microstructure. If the id equals 0, then the cell is empty and can be updated according to some fixed transition rules. If not – the element is assigned to n-th grain, where n is grain number. The neighbourhood is a set of cells related to a specified element of the grid, which are used to determine its id in the next step of the algorithm. Moreover, boundary conditions at the computational domain have to be specified, e.g., periodic or absorbent, respectively.

To initiate the cellular automata grain growth algorithm, the generated computational domain has to be discretized by the regular space of CA cells. In the paper, the geometry of each CA cell is a square in 2D and a cube in 3D space. The concept of the developed mapping algorithm of the closed packed shapes into the CA space is shown in figure 13.

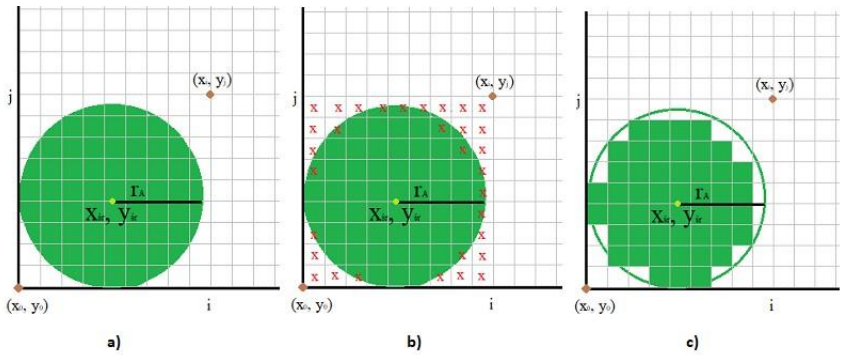

***Fig. 13**. Example of the mapping process for 2D space: a) geometrical description of the generated shape, b) identification of the overlapping area with CA spaces, c) conversion to the CA space.*

The same approach can be used to 2D and 3D computational domains, with appropriate conversion equations:

$$\left(x_i - x_{śr}\right)^2 + \left(y_j - y_{śr}\right)^2 < r^2 \quad (9)$$

$$\left(x_i - x_{śr}\right)^2 + \left(y_j - y_{śr}\right)^2 + \left(z_k - z_{śr}\right)^2 < r^2 \quad (10)$$

Finally, the CA grain growth model described in (Madej, 201) was implemented in this work to obtain the final digital microstructure model.

The computational domain is additionally split into *N* equally sized parts, which are processed separately by different threads to decrease the computational time of the developed algorithm. The applied method executes one of the loops "for", so each iteration may be run in parallel. The number of iterations that can run in parallel is set up according to the number of processors.

To check the influence of circles/spheres packing density on the final grain size distribution the input data from figure 7 - figure 12 after conversion were used during the CA growth stage. Examples of obtained results are shown in figures 14 - 19.

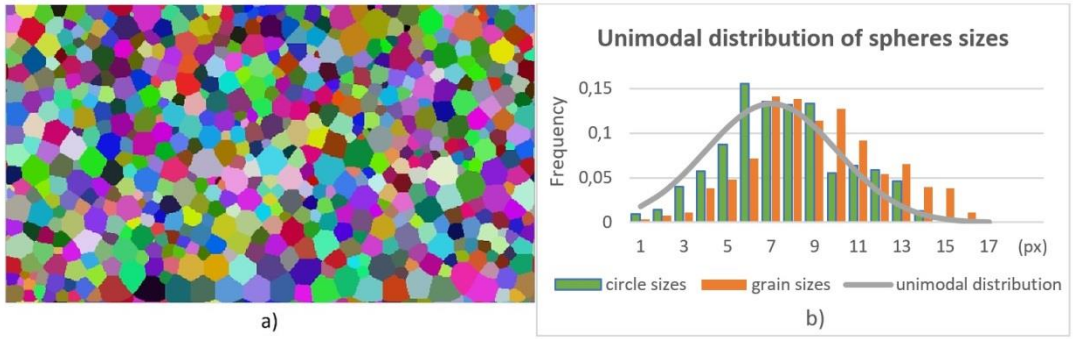

***Fig. 14**. Results for the unimodal distribution: a) 2D digital microstructure, b) comparison of the theoretical and obtained size distributions.*

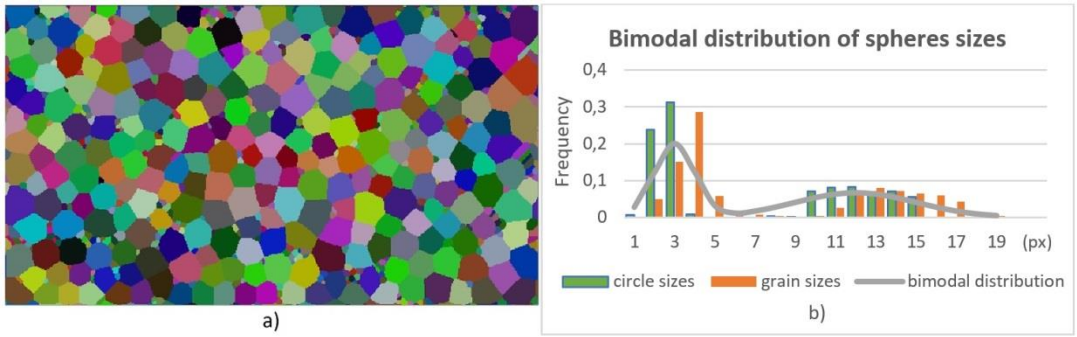

***Fig. 15**. Results for the bimodal distribution: a) 2D digital microstructure, b) comparison of the theoretical and obtained size distributions.*

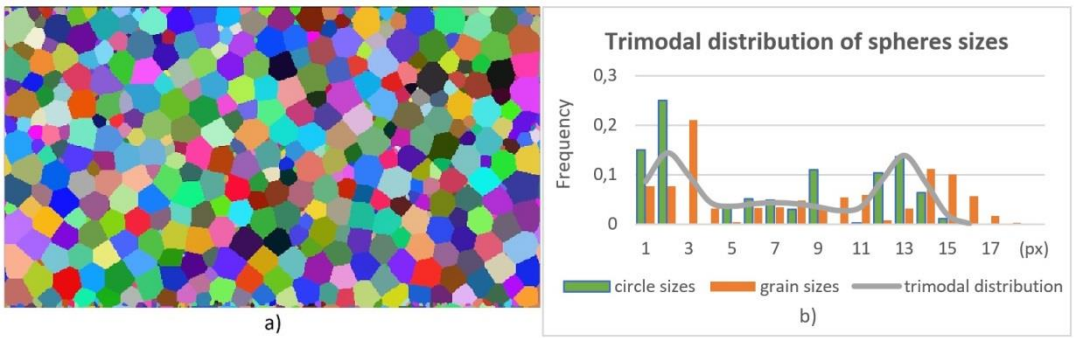

***Fig. 16**. Results for the trimodal distribution: a) 2D digital microstructure, b) comparison of the theoretical and obtained size distributions.*

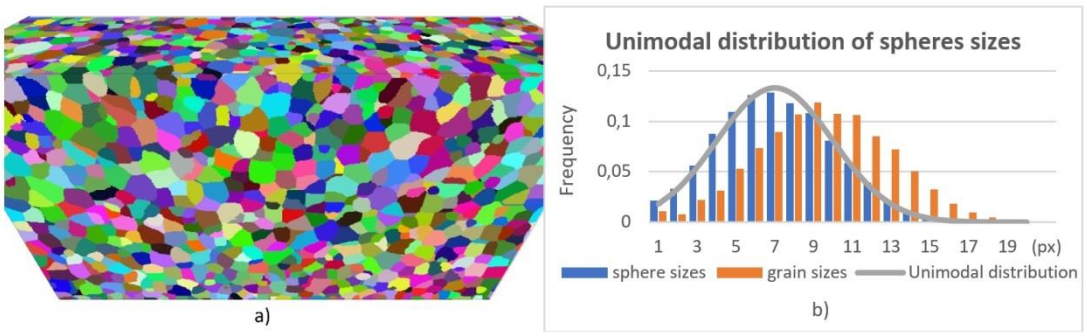

***Fig. 17**. Results for the unimodal distribution: a) 3D digital microstructure, b) comparison of the theoretical and obtained size distributions.*

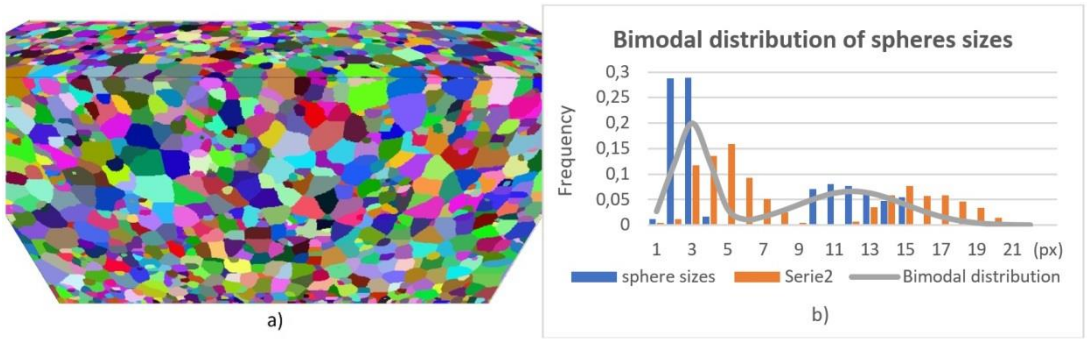

***Fig. 18**. Results for the bimodal distribution: a) 3D digital microstructure, b) comparison of the theoretical and obtained size distributions.*

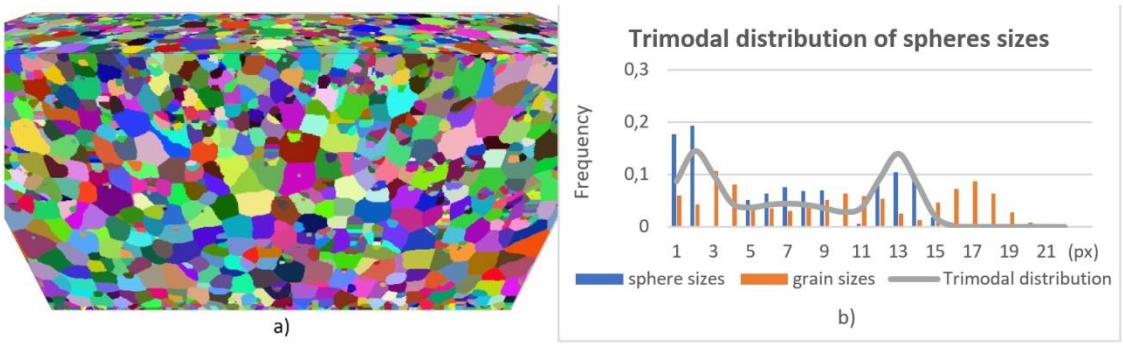

***Fig. 19**. Results for the trimodal distribution: a) 3D digital microstructure, b) comparison of the theoretical and obtained size distributions.*

As seen in each case study, the final grain sizes are larger than close-packed shapes sizes, because the initial domain is not filled in 100%. For tests 1, 2 and 3 (table 1), the packing density is at the level above 77%. The empty spaces occupy less than 23% of the computational domain; therefore, quite similar distributions after the CA grain growth algorithm were obtained. Unfortunately for 3D domains, only 45% of the computational domain is filled with 3D shapes, and after the grain growth, the discrepancies in the final grain size distributions are significant.

One of the approaches to overcome the issue with low packing density is to use optimization algorithms during the sphere packing stage as described in (Madej, et al., 2014). The other is the substitution of the spherical shape of objects by the elliptical ones. This will be the subject of future work.

As the model contains stochastic elements, to evaluate its robustness, the additional set of calculations was designed and executed. For this, each of the presented earlier case studies was recalculated ten times and compared with the appropriate distribution to confirm that the model provides repeatable results. Obtained data are summarized in the last column of table 3.

Presented results confirm that generated objects have dimensions within the range provided by the distribution. The number of objects for a given size was slightly different in each simulation, but it does not affect the overall model response.

Table 3*. Repeatability of results for the three case studies of the developed 2D and 3D version of the algorithm.*

Distribution	Range of radius, px	m, px	σ, px	Packing density, %
2D Unimodal	[1; 15]	8	3	88.5
2D Bimodal	[1; 5] [10; 15]	3 12	1 3	85.9
2D Trimodal	[1; 3] [5; 9] [12; 15]	2 7 13	1 3 1	84.2
3D Unimodal	[1; 15]	7	3	90.6
3D Bimodal	[1; 6] [10; 15]	3 12	3 1	94.5
3D Trimodal	[1; 3] [5; 9] [12; 15]	2 7 13	1 3 1	92.6

4. SUMMARY AND CONCLUSIONS

Based on the presented research, the following conclusions can be drawn:

1. The developed algorithm provides digital microstructures with three different grain size distributions: unimodal, bimodal and trimodal.
2. The algorithm with minor modifications can be used for generation of 2D and 3D digital models.
3. The 2D model provides satisfactory packing density that enables proper replication of required grain size.
4. The 3D model does not provide satisfactory packing density, therefore the obtained final grain size distributions can be far from expectations. This algorithm can be used mainly when the qualitative agreement is satisfactory.
5. The arrangement of the objects in the computational domain is random in each case however the repeatability of the results for a given case study is high even for the 2D space.

Implementation of the 3D algorithm operating on the ellipsoids instead of the spheres to overcome issues mentioned in the paper will be the subject of the future work.

ACKNOWLEDGMENTS

The work was realized as a part of fundamental research financed by the Ministry of Science and Higher Education, grant no. 16.16.110.663.

REFERENCES

Banhart, J., 2008, *Advanced tomographic methods in material research and engineering*, Oxford University Press.

Baranau, V., Tallarek, U., 2014, Random-close packing limits for monodisperse and polydisperse hard spheres, *Soft Matter*, 10(21), 3826-3841.

Clarke, A.S., Wiley, J.D., 1987. Numerical simulation of the dense random packing of a binary mixture of hard spheres: Amorphous metals, *Physical Review B*, 35(14), 7350-7356.

Cui, L., O'Sullivan, C., 2003, Analysis of a triangulation based approach for specimen generation for discrete element simulations, *Granul. Matter*, 5, 135-145.

Burnett, T.L., Polonsky A.T., Pollock, T.M., Withers P.J., 2020, Serial sectioning in the SEM for three dimensional materials science, *Current Opinion in Solid State and Materials Science*, 24(2), 100817.

Evans, J.W., 1993, Random and cooperative sequential adsorption, *Reviews of Modern Physics*, 65, 1281-1304.

Gawad, J., Madej, L., Szeliga, D., Pietrzyk, M., 2005, Cellular automaton technique as a tool for a complex analysis of the microstructure evolution and rheological behavior, *Acta Metallurgica Slovaka*, 11, 45-53.

He, K., Ye, H., Wang, Z., Liu, J., 2018, An efficient quasi-physical quasi-human algorithm for packing equal circles in a circular container, *Computers and Operations Research*, 92, 26 -36.

Hitti, K., Bernacki, M., 2013, Optimized dropping and rolling (ODR) method for packing of poly-disperse spheres, *Applied Mathematical Modelling*, 37(8), 5715-5722.

Hoffpauir, B.K., Pope, B.A., Spirou, G.A., 2007, Serial sectioning and electron microscopy of large tissue volumes for 3D analysis and reconstruction: a case study of the calyx of held, *Nature Protocols*, 2(1), 9-22.

Ilina, D.N., Bernacki, M., 2016, A new algorithm for dense ellipse packing and polygonal structures generation in context of FEM or DEM, *MATEC Web of Conferences*, vol. 80, doi: 10.1051/matecconf/20168002004.

Jodrey, W.S., Tory, E.M., 1979, Simulation of random packing of spheres, *Simulation*, 32(1), 1-12.

Kazakov, A.L., Lempert, A.A., Ta, T.T., 2018, The sphere packing problem into bounded containers in three-dimension non-Euclidean space, *IFAC-PapersOnLine*, 51(32), 782 -787.

Khirevich, S., Höltzel, A., Tallarek, U., 2013, Validation of pore-scale simulations of hydrodynamic dispersion in random sphere packings, *Communications in Computational Physics*, 13(3), 801-822.

Madej, L., 2017, Digital virtual microstructures in application to metals engineering - a review, *Archives of Civil and Mechanical Engineering*, 17, 839-854.

Madej, L., Pasternak, K., Szyndler, J., Wajda, W., 2014. Development of the modified cellular automata sphere growth model for creation of the digital material representations,. *Key Engineering Materials*, 611, 489-496.

Orick, G.L., Stephenson, K., Collins, C., 2017, A linearized circle packing algorithm, *Computational Geometry: Theory and Applications*, 64, 13-29.

Pietrzyk, M., Madej, L., Rauch, L., Szeliga, D., 2015, *Computational materials engineering: achieving high accurancy and efficiency in metals processing simulations*, Butterworth-Heinimann, Elsevier.

Raabe, D., Becker, R., 2000, Coupling of a crystal plasticity finitelement model with a probabilistic cellular automaton for simulating primary static recrystallization in aluminium, *Modelling and Simulation in Materials Science and Engineering*, 8, 445-462.

Romanova, T., Litvinchev, I., Pankratov, A., 2020, Packing ellipsoids in an optimized cylinder, *European Journal of Operational Research*, 285(2), 429 - 443.

Sahu, K., 2009, Gravity packing of same size spheres and investigation of wall ordering, *International Journal of Chemical Reactor Engineering*, 7(1), doi:10.2202/1542-6580.1932

Shi, Y., Zhang, Y., 2008, simulation of random packing of spherical particles with different size distributions, *Applied Physics A*, 92(3), 621-626.

Sitko, M., Mojzeszko, M., Rychlowski, L., Cios, G., Bala, P., Muszka, K., Madej, L., 2020. Numerical procedure of three-dimensional reconstruction of ferrite-pearlite microstructure data from SEM/EBSD serial sectioning, *Procedia Manufacturing*, 47, 1217 - 1222.

Sohn, H.Y., Sridhar, S., 2005. Description of high-temperature metallurgical processes, in: *Fundamentals of metallurgy*, Padstow: Woodhead Publishing Limited, 3-38.

Torquato, S., Jiao, Y., 2010, Robust algorithm to generate a diverse class of dense disordered and ordered sphere packings via linear programming, *Physical Review E*, 82(6), 061302.

Jodrey, W.S., Tory, E.M., 1986, Computer simulation of close random packing of equal spheres, *Physical Review A*, 32(4), 2347-2351.

Totten, G., Pye, D., 2004, *Heat-treating process design. in: handbook of metallurgical process design*, CRC Press, New York, 453 - 506.

Vásárhelyi, L., Kónya, Z., Kukovecz, Á., Vajtai, R., 2020, Microcomputed tomography–based characterization of advanced materials: a review, *Materials Today Advances*, 8, 100084, doi.org/10.1016/j.mtadv.2020.100084.

Visscher, W.M., Bolsterli, M., 1972, Random packing of equal and unequal spheres in two and three dimensions, *Nature*, 239, 504-507.

Von Neumann, J., 1966, Theory of self-reproducing automata, ed.., Burks, A.W., University of Illinois Press, Urbana, London.

ALGORYTM SPADAJĄCYCH SFER DLA GENERACJI CYFROWEJ REPREZENTACJI MODELU POLIKRYSTALICZNYCH MIKROSTRUKTUR Z HETEROGENICZNYMI ROZMIARAMI ZIAREN

Streszczenie

W pracy przedstawiono opracowanie algorytmu pakowania sferycznego automatu komórkowego (CA) dedykowanego do generowania dwu- i trójwymiarowych, cyfrowych, syntetycznych modeli mikrostruktury o niejednorodnym rozkładzie ziarnistości. Syntetyczny model mikrostruktury jest generowany w czterech głównych etapach: generowanie domeny obliczeniowej automatu komórkowego 2D/3D, generowanie okręgów/kul o wymaganym rozkładzie wielkości, wypełnianie domeny obliczeniowej wygenerowanymi okręgami/kulami, wzrost okręgów/kul zgodnie z algorytmem nieograniczonego wzrostu CA. W rezultacie otrzymujemy syntetyczne modele mikrostruktury o specyficznym, wymaganym rozkładzie uziarnienia opisanym np. jedno- lub dwumodalnym rozkładem. Aby zmniejszyć złożoność obliczeniową i skrócić czas wykonania, rotacja kół/kul podczas etapu pakowania opiera się na wektorowym rozliczaniu odległości od granic domen obliczeniowych z innymi sferami. Algorytm wzrostu ziarna CA jest również zaimplementowany z wykorzystaniem mechanizmu wątków, co pozwala na równoległe wykonywanie obliczeń w celu zwiększenia jego wydajności. W artykule przedstawiono opracowany algorytm wraz ze szczegółami implementacji oraz zestawem przykładów uzyskanych wyników.

Received: April 1 2020.
Received in a revised form: July 1 2020.
Accepted: July 21 2020.